

Nonlinear axion dynamics and the formation of cosmological pseudosolitons

Edward W. Kolb*

*NASA/Fermilab Astrophysics Center, Fermi National Accelerator Laboratory, Batavia, Illinois 60510
and Department of Astronomy and Astrophysics, Enrico Fermi Institute, The University of Chicago, Chicago, Illinois 60637*

Igor I. Tkachev†

*NASA/Fermilab Astrophysics Center, Fermi National Accelerator Laboratory, Batavia, Illinois 60510
and Institute for Nuclear Research of the Academy of Sciences of Russia, Moscow 117312, Russia*

(Received 18 November 1993)

The (3+1)-dimensional evolution of an inhomogeneous axion field configuration around the QCD epoch is studied numerically, including important nonlinear effects due to the attractive self-interaction. It is found that axion perturbations on scales corresponding to causally disconnected regions at $T \sim 1$ GeV can lead to very dense pseudosoliton configurations we call axitons. These configurations evolve to axion miniclusters with a present density $\rho_a \gtrsim 10^{-8}$ g cm $^{-3}$. This is high enough for the collisional $2a \rightarrow 2a$ process to lead to Bose-Einstein relaxation in the gravitationally bound clumps of axions, forming Bose stars.

PACS number(s): 98.80.Cq, 05.30.Jp, 14.80.Mz, 98.70.-f

I. INTRODUCTION

The invisible axion is one of the best motivated candidates for cosmic dark matter. The axion is the pseudo Nambu-Goldstone boson resulting from the spontaneous breaking of a U(1) global symmetry known as the Peccei-Quinn (PQ) symmetry. The PQ symmetry is introduced to explain the apparent smallness of strong CP violation in QCD [1]. Although there are other possible solutions to the strong CP problem [2], and the origin of the axion in the breaking of a *global* symmetry has been criticized [3], the axion remains the best known cure for the disease of strong- CP violation.

There are stringent astrophysical [4,5] and cosmological [6] constraints on the properties of the axion. In particular, the combination of cosmological and astrophysical considerations restrict the axion decay constant f_a and the axion mass m_a to be in the narrow windows 10^{10} GeV $\lesssim f_a \lesssim 10^{12}$ GeV, and 10^{-5} eV $\lesssim m_a \lesssim 10^{-3}$ eV [7]. The contribution to the mean density of the Universe from axions with mass in this window is guaranteed to be cosmologically significant. Thus, if axions exist, they will be dynamically important in the present evolution of the Universe.

In addition to the usual role in the evolution of primordial density fluctuations and the formation of large-scale structure common to all cold dark matter candidates, axions have unique features as dark matter. The energy density in axions corresponds to coherent scalar field oscillations, driven by a displacement of the initial value of the field (the “misalignment” angle) away from the eventual minimum of the temperature-dependent potential.

During the QCD epoch fluctuations in the misalignment angle on scales comparable to the Hubble radius at that time [8] are transformed into large amplitude density fluctuations, which later lead to tiny gravitationally bound “miniclusters” [9]. It was found that the density in miniclusters exceeds by ten orders of magnitude the local dark matter density in the solar neighborhood [9]. This might have a number of astrophysical consequences, as well as implications for laboratory axion searches [10].

In previous studies of the evolution of the axion field around the QCD epoch, the effect of spatial gradients of the axion field were either neglected, or were included in a limit where the nonlinear potential was approximated by a *linear* harmonic potential. Both approximations are adequate for temperatures well below the QCD scale where the coherent axion oscillations can be treated as pressureless, cold dust. However, in a previous paper [11] we found that just at the crucial time when the inverse mass of the axion is approximately the size of the Hubble radius and fluctuations of misalignment angle are still of order π , both the nonlinear interaction and the gradient terms are important, and a full field-theoretical calculation is needed. Here we present the results of a three-dimensional numerical study of the evolution of the inhomogeneous axion field around the QCD epoch. We find that the resulting axion clumps are much denser than previously thought, even reaching the critical conditions for Bose star formation [12].

In Sec. II we review the basic scenario for the evolution of the axion field around the QCD epoch. In Sec. III, after deriving the equations of motions in a suitable form, we present the results of (3+1)-dimensional numerical calculations of an initial white-noise axion distribution. We find that the nonlinear potential leads to the formation of dense, roughly spherical, solitonlike axion configurations we call axitons. We then follow the subsequent evolution of these spherically symmetric configurations in a (1+1)-dimensional calculation. Sec-

*Electronic address: rocky@fnas01.fnal.gov

†Electronic address: tkachev@fnas13.fnal.gov

tion IV is devoted to the consideration of an initial axion field that results in a network of topological defects. We discuss how the usual picture of axion strings slicing up axion domain walls is modified by the inclusion of the nonlinearities of the true axion potential. We find that rather than the simple picture of axion strings destroying walls by punching holes in them, unstable pseudobreather solitons are formed which decay to axitons. In the final section we discuss some possible physical consequences of very dense axion clumps.

II. COSMOLOGICAL EVOLUTION OF THE AXION FIELD

The axion story begins with PQ symmetry breaking. This symmetry breaking occurs when a complex scalar field ϕ with nonzero PQ charge develops a vacuum expectation value. This PQ symmetry breaking can be modeled by considering a potential of the standard form $V(\phi) = \lambda(|\phi|^2 - f_a^2/2)^2$. The axion is the resulting Nambu-Goldstone degree of freedom from spontaneous breaking of the global symmetry. After PQ symmetry breaking at $T \sim f_a$, but before QCD effects are important, the axion is massless. However since the PQ symmetry is anomalous, it is broken explicitly by QCD instanton effects, leading to a mass for the axion. In general the instanton effects respect a residual Z_N symmetry, and the axion develops a potential due to instanton effects of the form $V(a) = m_a^2 (f_a/N)^2 [1 - \cos(Na/f_a)]$. The axion field is often represented in terms of an angular variable $\theta \equiv Na/f_a$, and if θ is taken as the dynamical variable, its potential for $N = 1$ is

$$\begin{aligned} V(\theta) &= m_a^2(T) f_a^2 (1 - \cos\theta) \\ &\equiv \Lambda_a^4(T) (1 - \cos\theta). \end{aligned} \quad (2.1)$$

Because QCD instantons are large, with a size set by $\Lambda_{\text{QCD}}^{-1}$, their effects are strongly suppressed at high temperatures. So for $T \gg \Lambda_{\text{QCD}}$, the axions are effectively massless. For $T \gg \Lambda_{\text{QCD}}$, the temperature dependence of the axion mass scales as [13,8]

$$m_a^2(T) = m_a^2(T_*) (T/T_*)^{-n}, \quad n = 7.4 \pm 0.2. \quad (2.2)$$

When the field $\theta(x)$ is created during the Peccei-Quinn symmetry-breaking phase transition at $T \sim f_a$, it should be uncorrelated on scales larger than the Hubble radius at that time [14]. As the temperature decreases and the Hubble radius grows [in a radiation-dominated universe the Hubble radius grows as $R_H(T) \equiv H^{-1}(T) \propto T^{-2}$], the field becomes smooth on scales up to the Hubble radius. This continues until $T = T_1 \sim 1$ GeV when the axion mass “switches on,” i.e., when $m_a(T_1) \approx 3H(T_1)$, and the axion mass begins to become important in the equations of motion. Coherent axion oscillations then transform fluctuations in the initial amplitude of the axion field into fluctuations in the axion density.

Since the initial amplitude of the coherent axion oscillations on the scale of the Hubble radius is uncorrelated, one expects that typical positive density fluctuations on this scale will satisfy $\rho_a \approx 2\bar{\rho}_a$, where $\bar{\rho}_a$ is mean cosmo-

logical density of axions [9]. At the temperature of equal matter and radiation energy density, $T_{\text{eq}} = 5.5 \Omega_a h^2 \text{ eV}$ [15], nonlinear fluctuations will separate out as miniclusters with $\rho_{\text{mc}} \approx 10^{-14} \text{ g cm}^{-3}$ [9]. The minicluster mass will be of the order of the axion mass within the Hubble radius at temperature T_1 , $M_{\text{mc}} \sim 10^{-9} M_\odot$. The radius of the cluster is $R_{\text{mc}} \sim 10^{13} \text{ cm}$, and the gravitational binding energy will result in an escape velocity of $v_e/c \sim 10^{-8}$. Note that the mean phase-space density of axions in such a gravitational well is enormous: $\bar{n} \sim \rho_a m_a^{-4} v_e^{-3} \sim 10^{48} f_{12}^4$, where $f_{12} \equiv f_a/10^{12} \text{ GeV}$.

We will show below that due to nonlinear effects, a substantial number of regions at $\Lambda_{\text{QCD}} > T > T_{\text{eq}}$ can have an axion density orders of magnitude larger than $2\bar{\rho}_a$. These form because the nonlinear effects in the axion potential lead to the formation of pseudosoliton objects we call axitons.

The axitons are not true solitons because the field coherently oscillates inside the axiton. The oscillations of the field lead to a redshift of the energy density of the field in an expanding universe. Quantitatively, axitons resemble breathers of the (1+1)-dimensional sine-Gordon model.

Eventually the energy density of the axiton is redshifted to sufficiently small values of the axion field so that nonlinearities can be neglected, and the axiton configuration is frozen in the cosmological expansion as is any linear fluctuation. However the energy contrast relative to the homogeneous background will be large.

Once an axiton forms, its energy density scales as T^3 for $T > T_{\text{eq}}$, so we can write $\rho_{\text{axiton}} \equiv 3(1 + \Phi)T_{\text{eq}}^3 s/4$, where Φ depends upon the initial conditions of the axion field, i.e., the misalignment angle and its gradients at T_1 . Here, s is the entropy density, and $\Phi = 0$ corresponds to the mean axion density. The energy density excess inside a given fluctuation is equal to the radiation energy density at $T = \Phi T_{\text{eq}}$. At that time the self-gravity of the fluctuation comes to dominate, and if $\Phi \gtrsim 1$ it separates out from the cosmological expansion, collapses, and forms a minicluster with a density¹

$$\begin{aligned} \rho_{\text{mc}} &\approx 140 \Phi^3 (1 + \Phi) \bar{\rho}_a (T_{\text{eq}}) \\ &\approx 3 \times 10^{-14} \Phi^3 (1 + \Phi) (\Omega_a h^2)^4 \text{ g cm}^{-3}. \end{aligned} \quad (2.3)$$

Even a relatively small increase in Φ is important because the final density depends upon Φ^4 .

Ours is not the first proposal that nonlinear effects can lead to large values of Φ . One mechanism whereby nonlinear effects can lead to amplification of the axion density was recognized in Ref. [8]. In that analysis it was proposed that some correlation regions can have values of Φ larger than one because the closer the initial value of θ is to the top of the axion potential, the later axion oscillations commence. However, this effect alone is not very significant. If the closeness of the initial angle to the top of the potential is parametrized by $\xi \equiv (\pi - \theta_i)/\pi$, then

¹The factor of 140 results from a detailed calculation.

for ξ in the range $0.1 \lesssim \xi \lesssim 10^{-3}$, we can fit the numerical results of the Ref. [8] by the formula $\Phi - 1 \approx 1.5(\theta_i/\pi)^2 \xi^{-0.35}$. This regime was studied also in Ref. [16] analytically. We see that Φ is significantly larger than 1 only for initial values very finely tuned to the top of the potential [11]. Moreover, the axion field is not exactly coherent on scales of the Hubble radius, and even small fluctuations will spoil this simple picture.

Our scenario for the generation of axion miniclusters mainly depends upon the interplay of the nonlinear effects in the potential and gradients in the axion field. The interplay of these two effects will lead to the formation of axion configurations in the axion field. At temperatures $T \gg T_1$, the potential is negligible in the equations of motion compared to the gradient terms which force the field to be homogeneous on scales less than the Hubble radius. At $T \ll \Lambda_{\text{QCD}}$, gradients can be neglected and one can treat the evolution of fluctuations as that of a pressureless gas. Clearly, around the QCD epoch when the potential just starts to become important in the equations of motion the gradient terms are still important, and since the initial amplitude can be close to π , the nonlinear nature of the potential is also important. In order to find the energy density profile at freeze-out one has to trace the nonlinear inhomogeneous field evolution through the epoch $T \sim T_1$.

III. INHOMOGENEOUS AXION FIELD EVOLUTION

A. Equations of motion

We start with deriving the equations of motion for the axion field in a form suitable for numerical calculations. In an expanding, spatially flat universe with scale factor $R(t)$, the equation of motion for the axion field takes the familiar form

$$\ddot{\theta} + 3 \frac{\dot{R}}{R} \dot{\theta} - \frac{1}{R^2(t)} \bar{\Delta} \theta + m_a^2(t) \sin \theta = 0, \quad (3.1)$$

where an overdot denotes a time derivative and $\bar{\Delta}$ is the Laplacian with respect to comoving coordinates \bar{x} .

Rather than cosmological time, it is convenient to work with a conformal-time coordinate. In a radiation-dominated universe the conformal time is proportional to the scale factor R . Using R as the independent variable, the equation of motion is

$$\frac{d^2 \theta}{dR^2} + \frac{2}{R} \frac{d\theta}{dR} - \frac{1}{\dot{R}^2} \frac{1}{R^2(t)} \bar{\Delta} \theta + \frac{1}{\dot{R}^2} m_a^2(R) \sin \theta = 0. \quad (3.2)$$

Using the Friedmann equation, along with the dependence of the expansion rate upon R in a radiation-dominated universe, we can express \dot{R}^2 in terms of the Hubble radius at some arbitrary epoch (denoted by subscript 1): $\dot{R}^2 = H^2 R^2 = H^2(R_1) R_1^4 / R^2$. Now defining conformal time η as $\eta \equiv R / R_1$, the equation of motion is

$$\theta'' + \frac{2}{\eta} \theta' - \frac{1}{H^2(R_1) R_1^4} \bar{\Delta} \theta + \frac{\eta^2}{H^2(R_1)} m_a^2(R) \sin \theta = 0, \quad (3.3)$$

where a prime denotes $d/d\eta$. We use Eq. (2.2) to find that in conformal time the mass evolves as $m_a^2(R) = m_a^2(R_1) \eta^n$. We can use the remaining freedom in the choice of R_1 to simplify the equation of motion by making the choice $m_a^2(R_1) = H^2(R_1)$, i.e., $\eta = 1$ corresponds to the epoch when the inverse of the axion mass is equal to the Hubble radius. The equation of motion then takes the form

$$\theta'' + \frac{2}{\eta} \theta' - \Delta \theta + \eta^{n+2} \sin \theta = 0, \quad (3.4)$$

where Δ is now the Laplacian with respect to comoving coordinates, $x \equiv H(R_1) R_1 \bar{x}$. In other words, $x = 1$ corresponds to the Hubble radius at the epoch when the Hubble radius is the inverse of the axion mass.

The equation of motion can be written as a wave equation by the introduction of the field $\psi \equiv \eta \theta$:

$$\psi'' - \Delta \psi + \eta^{n+3} \sin(\psi/\eta) = 0. \quad (3.5)$$

The equation of motion is finally in a form convenient for the study of the evolution of the axion field during the epoch when the mass switches on. In Table I we give the scaling with η of several important physical length and mass scales. We next turn to the specification of the initial conditions.

B. Initial conditions

At $\eta \ll 1$ the potential term in Eq. (3.5) can be neglected, and the solution of the wave equation can be expressed simply as a sum of Fourier harmonics. As usual, there will be two sums over frequency ω : one sum proportional to $\sin(\omega\eta)$ and one sum proportional to $\cos(\omega\eta)$. In the decomposition of the θ field, terms such as $A(\omega) \sin(\omega\eta)/(\omega\eta)$ and $B(\omega) \cos(\omega\eta)/(\omega\eta)$ will appear. Assuming a finite amplitude for fluctuations of θ (of order of several π) on scales larger than the Hubble radius at the epoch of the Peccei-Quinn phase transition, we see that the coefficients $B(\omega)$ must be proportional to Λ_{QCD}/f_a , while the coefficients $A(\omega)$ are of order unity. In other words the terms proportional to $\cos(\omega\eta)$ correspond to decaying modes on scales larger than the Hubble radius and can be neglected. Finally, assuming that on large scales the distribution for θ is white noise, we obtain

$$\theta = A \pi \sum_{ijk} \frac{\sin(\omega\eta)}{\omega\eta} \sin(p_i x + \varphi_{1ijk}) \sin(p_j y + \varphi_{2ijk}) \times \sin(p_k z + \varphi_{3ijk}), \quad (3.6)$$

TABLE I. The scaling of physical quantities with conformal time η . To find the scaling in coordinate distance, a length must be divided by η , and a mass multiplied by η .

Time	$t(\eta) = t(\eta=1) \eta^2$
Temperature	$T(\eta) = T(\eta=1) \eta^{-1}$
Scale factor	$R(\eta) = R(\eta=1) \eta$
Axion mass	$m_a(\eta) = m_a(\eta=1) \eta^{n/2}$ $n = 7.4 \pm 0.2$
Hubble radius	$R_H(\eta) \equiv H^{-1}(\eta) = R_H(\eta=1) \eta^2$

where φ 's are random phases and $\omega^2 = p_i^2 + p_j^2 + p_k^2$. On scales larger than the Hubble radius the field distribution is frozen, while modes smaller than the Hubble radius are redshifted away.

We numerically evolved this distribution starting from initial time $\eta = 0.4$ in a box of size $L = 4$ with periodic boundary conditions. There were 100^3 grid points in the box. Each of the momenta in the field decomposition took six discrete values, $p_n = 2\pi n / L$, with $n = 1, \dots, 6$. So, in total there were 3×6^3 random phases, each with values in the interval $0 < \varphi < 2\pi$.

The final parameter to be chosen is the magnitude of A . Recall that for $N = 1$, the axion potential is periodic with period 2π . We will consider two possibilities: $A = 1$ and $A = 2$. For the case $A = 1$ it is unlikely that domain walls will form in a box of the size we study. However for $A = 2$ (the more physical choice) domain walls are produced at about 1 per horizon. We will present some results where $A = 2$, but for the most part we will consider in detail calculations with the $A = 1$ initial condition, since we are interested in the structure of density enhancements that are not associated with axion domain walls. So unless otherwise specified, our results will be for $A = 1$.

The initial conditions are illustrated in Fig. 1 by a two-dimensional slice through the three-dimensional box. The height above the plane is proportional to the axion energy density. Since at this epoch the axions are relativistic, it is convenient to scale their energy density by η^4 . The energy density shown in Fig. 1 is scaled by $\eta^4 / \bar{\rho}_a(\eta = 3)$ where $\bar{\rho}_a(\eta)$ represents mean axion energy density at a given η . Note that the Hubble radius at this epoch ($\eta = 0.4$) is 0.4 in the units of the figure, and the inverse of the axion mass is 75 units.

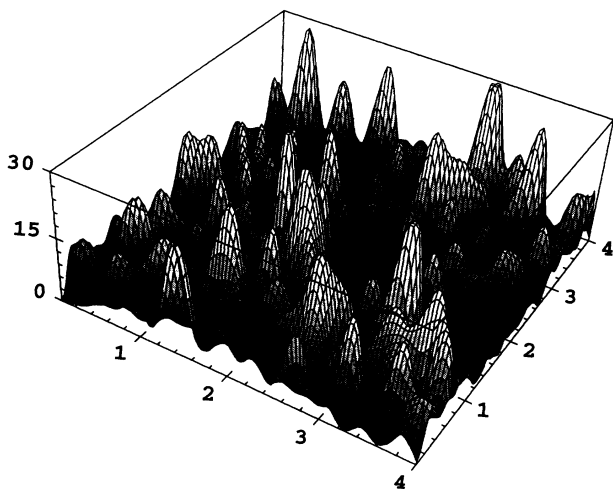


FIG. 1. A two-dimensional slice through the three-dimensional initial conditions for the axion field evolution. The time is $\eta = 0.4$. In the units shown in the figure the Hubble radius at this time is 0.4 units and the inverse of the axion mass is 75 units. The height of the figure corresponds to the energy density in the axion field: $\rho_a(\eta) \times \eta^4 / \bar{\rho}_a(\eta = 3)$.

C. Results of numerical calculations

1. (3+1)-dimensional evolution

We first present the results of numerical calculations with $A = 1$, where density peaks arising from collapsing domain walls are filtered out so as to isolate the effects due to axitons. In order to present the results of the calculations we will take a two-dimensional slice through the three-dimensional box, and plot the energy density as the height above the plane. We have analyzed the time evolution of the energy density in several different slices. All of the slices generally look alike. The most important (and generic) feature is the development of large-amplitude peaks. As the system evolves in time, the peaks in the energy density, the axitons, increase in magnitude and become more compact. We present the results in the $z = \text{const}$ plane, which intersects the point with the maximum energy density at the end of the calculation. We emphasize that all slices through the box are quantitatively similar. We normalize the energy density by comparing it to the energy density of a homogeneous axion field, $\bar{\rho}_a(\eta)$, with initial amplitude equal to the rms value of the misalignment angle, $\theta_{\text{rms}} = \pi / \sqrt{3}$.

In order to isolate the effect of the nonlinearities in the axion potential we also evolve the same initial conditions with a harmonic axion potential, $V(\theta) = m^2(T)f^2\theta^2/2$, and compare the evolution of the harmonic potential model to the axion model.

The distribution of the axion energy density in the reference plane (which is the same as in Fig. 1) at time corresponding to $\eta = 2$ is shown in Fig. 2(a) for the harmonic potential, and in Fig. 2(b) for the axion potential. The maximum energy density peak that picks the reference plane is clearly seen in Fig. 2(b) its top portion is chopped off to fit overall the scale of the figure.

The distribution of the axion energy density in the reference plane at time corresponding to $\eta = 3$ is shown in Fig. 3(a) for the harmonic potential, and in Fig. 3(b) for the axion potential. Again, the tops of the four peaks in Fig. 3(b) are chopped off; their height are in excess of 100. Of course the peaks are only evident for the axion potential model.

Comparing Fig. 3(b) to Fig. 2(b) we see that for the axion potential most of the high magnitude peaks grow considerably in height and became thinner, while most of the low amplitude peaks remain almost unchanged; i.e., they are in the linear regime and consequently are frozen by the cosmological expansion. There are some peaks (some even relatively high at $\eta = 2$) which decreased in amplitude. Those peaks represent the tails of the density clumps which reach their maximum at some other value of z . All high density peaks contract in the coordinate volume, those which decreased in height simply moved out of our reference plane. High density peaks do not develop in the evolution of the harmonic potential, and the evolution proceeds as was assumed in the linear analysis [8,9].

There is insufficient resolution on this grid to proceed further in time with the axion potential, but the harmonic potential can be evolved further. In Fig. 4 we present the

result of the distribution of the axion energy density in the reference plane at time corresponding to $\eta=4$ for the harmonic potential to demonstrate that as expected the evolution of the field in the linear regime is frozen by $\eta=3$. Note that the typical magnitude of the peaks is about 2 for the harmonic potential.

There is a simple, heuristic explanation for the fact that nonlinear effects lead to the formation of high density peaks. The average pressure over a period of homogeneous axion oscillations in the axion potential is negative,² and is equal to $\langle P \rangle \simeq -\Lambda_a^4(T)\theta_0^4/64$, where θ_0 is the amplitude of the oscillations [17] (this formula is val-

id for $\theta_0 \ll \pi$; as $\theta_0 \rightarrow \pi$, the field spends more and more time near the top of the potential, and $\langle P \rangle \rightarrow -2\Lambda_a^4$). In other words, the axion self-interaction is attractive. The larger the amplitude of oscillations inside the fluctuation, the more negative the pressure inside, and consequently, fluctuations with excess axions will contract in the comoving volume. In addition, matter with a smaller pressure suffers less redshift in cosmological expansion.

Before continuing our exploration of the evolution of the peaks by means of a one-dimensional calculation, we present some results of calculations with $A=2$, where domain walls are much more likely to form than the above calculation with $A=1$. The best way to illustrate the presence of domain walls is by a contour graph, where the shading represents the amplitude of the axion energy density. We show a graph of the energy density distributions for the axion potential at time $\eta=2$ with $A=2$ in Fig. 5(a) and compare it to a similar contour

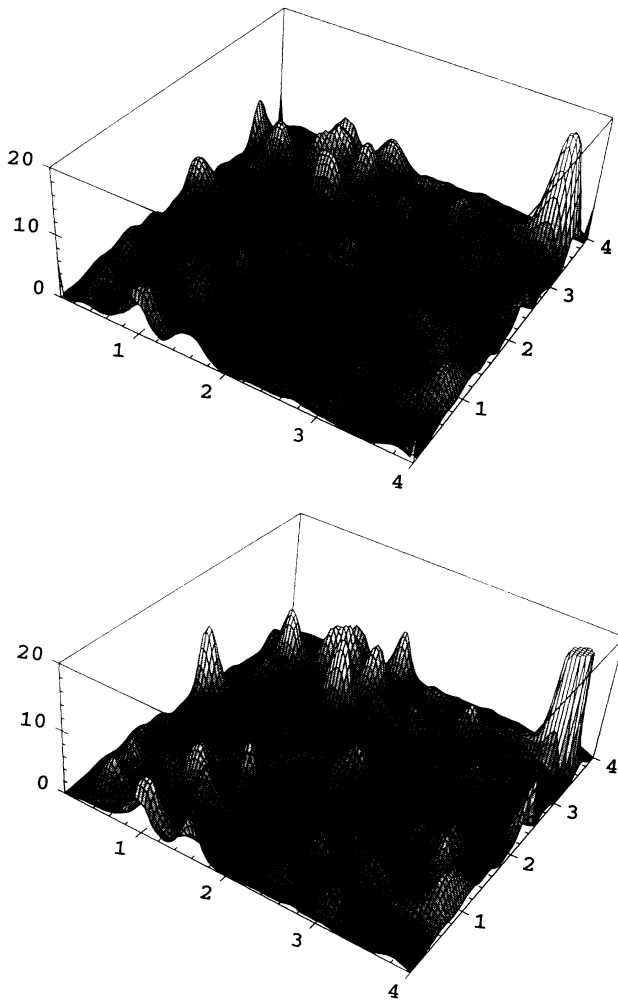


FIG. 2. A two-dimensional slice through the three-dimensional box at time corresponding to $\eta=2$ for the harmonic potential (top) and the axion potential (lower). The Hubble radius at this time is 2 units and the inverse of the axion mass is 0.038 units. The height of the figure corresponds to the energy density in the axion field normalized to the height for homogeneous field evolution: $\rho_a(\eta=2)/\bar{\rho}_a(\eta=2)$.

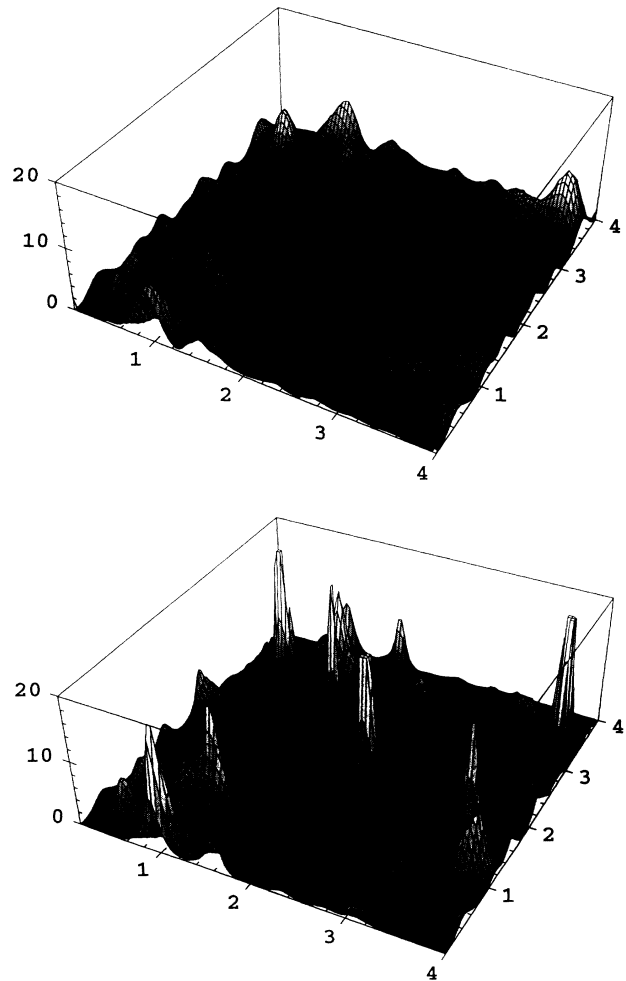


FIG. 3. A two-dimensional slice through the three-dimensional box at time corresponding to $\eta=3$ for the harmonic potential (top) and the axion potential (lower). The Hubble radius at this time is 3 units and the inverse of the axion mass is 0.005 units. The height of the figure corresponds to the energy density in the axion field normalized to the height for homogeneous field evolution: $\rho_a(\eta=3)/\bar{\rho}_a(\eta=3)$.

²Of course the average pressure is dominated by relativistic species at this time. It is the pressure contributed by the axions that is negative.

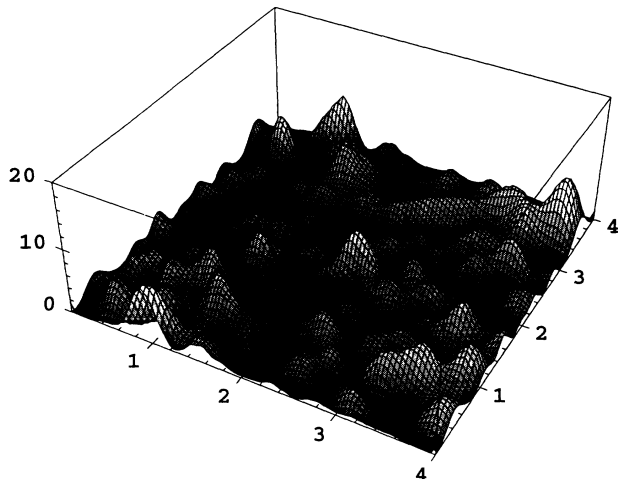


FIG. 4. A two-dimensional slice through the three-dimensional box at time corresponding to $\eta=4$ for the harmonic potential. The Hubble radius at this time is 4 units and the inverse of the axion mass is 0.0015 units. The height of the figure corresponds to the energy density in the axion field normalized to the height for homogeneous field evolution: $\rho_a(\eta=4)/\bar{\rho}_a(\eta=4)$.

graph for $A=1$ at $\eta=3$ in Fig. 5(b). In Fig. 5(a) two shells of collapsing domain walls are clearly visible in the lower left-hand corner and in the upper right-hand corner. Such configurations do not appear in Fig. 5(b). The density peaks in Fig. 3(b), the axitons, are not related to axion domain walls.

In order to learn the fate of the high density peaks, we have chosen one of them in Fig. 3 and generated the corresponding spherically symmetric initial conditions at $\eta=0.4$ and evolved it in time. We now describe the result of this calculation.

2. (1+1)-dimensional evolution

The axiton we choose to examine is the one near the center of the grid of Fig. 3, with grid coordinates $\{2.24, 1.92\}$ (the grid coordinate of the plane of Fig. 3 in the z direction is 1.76, also near the center of the three-dimensional box, and the axiton we chose is almost at its maximum in this plane, having an absolute maximum at $z=1.80$).

The dependence of the axion field upon time at the reference point at the center of this peak in our (3+1)-dimensional numerical calculation is shown in Fig. 6 by the solid curve. We can compare this evolution to the evolution of a massless axion field with the same initial conditions since we are able to calculate its evolution analytically from the massless wave equation with initial conditions given by Eq. (3.6). The evolution of a massless field at the reference point is shown in the Fig. 6 by the dashed line.

It is then straightforward to construct a spherically symmetric solution to the massless counterpart of Eq. (3.5) which has exactly the same time dependence as Fig. 6 in the center of the configuration. We start with the

field decomposition, Eq. (3.6), substitute the values of the coordinates of the given spatial point, and multiply each time harmonic by $\sin(\omega r)/\omega r$. So the dashed line in Fig. 6 also represents the time dependence for a massless field at the reference point of the (3+1)-dimensional calculation and also at the center of a (1+1)-dimensional spherically symmetric configuration. [Away from the reference point even the massless field will evolve differently in the (1+1)-dimensional calculation and the (3+1)-dimensional calculation.] We can use the resulting

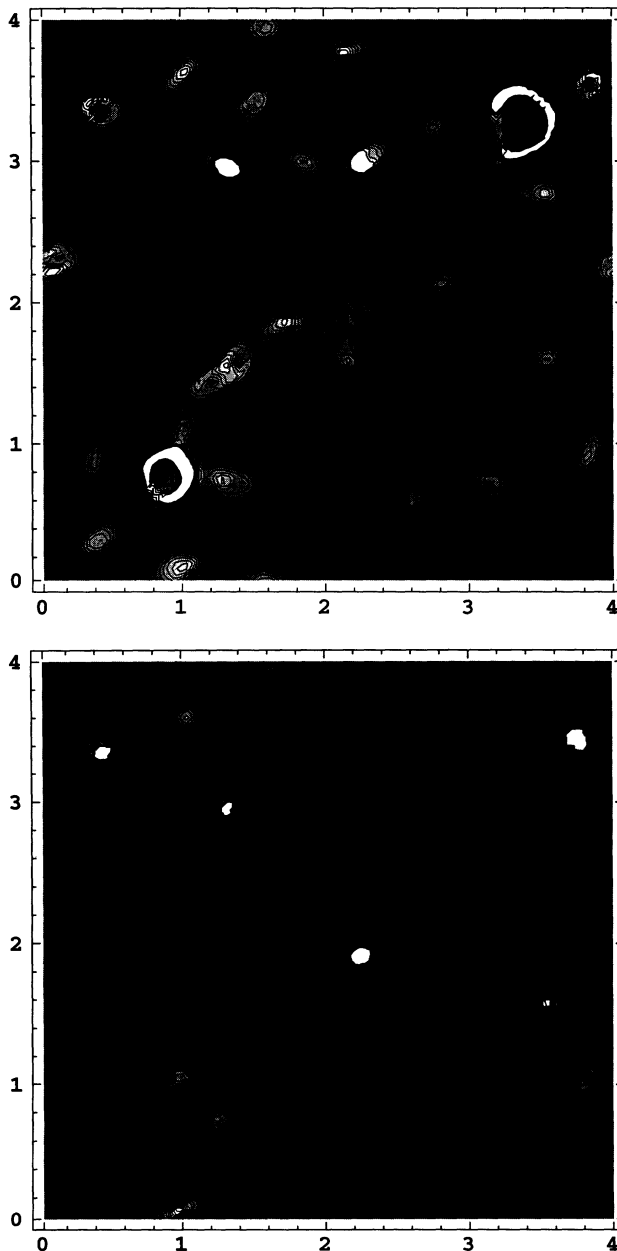


FIG. 5. A two-dimensional slice through the three-dimensional box. White regions correspond to high density. The upper figure is for $A=2$ at time corresponding to $\eta=2$ and the lower figure is for $A=1$ at $\eta=3$ [i.e., the same as in Fig. 3(b)].

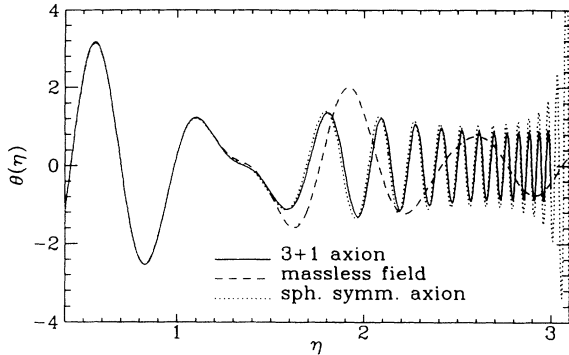


FIG. 6. Time dependence of the axion field at the center of an axiton. The solid curve is the result of the full (3+1)-dimensional calculation. The dashed curve is an analytic calculation for a massless field with the same initial conditions. The dotted curve is the (1+1)-dimensional calculation assuming spherical symmetry.

configuration $\theta = \theta(\eta, r)$ for generating spherically symmetric initial conditions which will approximate the peak of our choice for the runs with the actual axion potential. The result of such a calculation with $A = 1$ is shown in Fig. 6 by the dotted line.

This plot is instructive in the evaluation of the accuracy of the numerical code. At $\eta \lesssim 1$ the axion field is approximately massless, and the dotted curve is indistinguishable from the dashed curve (there were 10^4 grid points in the r direction in the case of spherical symmetry) and the solid curve deviates only very slightly (near the extrema) from the dashed curve. This suggests that the use of 100 grid points in each spatial direction in the (3+1)-dimensional calculations is adequate.

From Fig. 6 we see that the axion mass effectively switches on at a time $\eta \sim 1.3$. By this time the amplitude of the massless field is greater than unity.³ This means that for the evolution of the field using the axion potential the oscillations start in the nonlinear regime $\theta \gtrsim 1$ in the region that will develop into an axiton. We see also that the nonlinearity is strong enough to force the density peak to collapse not only in coordinate space, but also in physical space as well, since by the time $\eta \sim 3$ the amplitude of axion field oscillations are in the nonlinear regime and growing [this is somewhat difficult to see in the figure for a (3+1)-dimensional calculation]. The rate of growth in the nonspherical case is much slower (compare the solid and dotted lines). This makes sense because we expect a spherical collapse to lead to a denser central region.

So, in general, there are two competing effects in the evolution of the axion field: (1) a contraction of the axiton due to the pressure difference, leading to an increase

³Note that around $\eta = 2$ the amplitude for the massless calculation is slightly larger than the amplitude of the calculations using the true axion potential. This is because as the axion mass switches on the amplitude of the axion field decreases.

in amplitude in the center and (2) a decrease in amplitude of the oscillations due to the expansion of the Universe. We found that with a sufficiently large initial amplitude at the start of oscillations, the first process wins, and the amplitude in the center of the axiton increases to values $\theta \gtrsim \pi$. In the opposite case, e.g., if the initial amplitude when oscillations commence is in the linear regime, the amplitude monotonically decreases in time.

In realistic axion models the axion mass does not continue to grow with η , but saturates at its zero-temperature value around $T \sim \Lambda_{\text{QCD}}$. For axion masses in the allowed window this corresponds to $\eta \gtrsim 6$. Because of the steep power-law dependence of the function $m(\eta)$ in Eq. (2.2), the period of the field oscillations becomes very small by $\eta \sim 6$, and direct numerical methods fail even in the case of spherical symmetry. In order to follow the evolution of the fluctuation up to freeze-out we must assume that the mass saturates at a smaller value of η . This would correspond to a larger value of f_a . We have approximated the process of axion mass saturation by the simple formula

$$m^2(\eta) = m_a^2(\eta = 1)\eta^n / [1 + (\eta/\eta_c)^n], \quad (3.7)$$

taking $\eta_c = 3.5$. This value of η_c corresponds to too large a value of $f_a \sim 4 \times 10^{13}$ GeV, which would give $\Omega_a h^2$ in excess of one. However we expect that qualitatively the evolution of the axion field will have the same basic properties for larger values of η_c (the smaller values of f_a).

We can vary the initial overall amplitude A of our spherically symmetric configurations. This has the effect of spanning different initial conditions of a well-defined one-parameter family of axitons. Moreover, varying A is easier than choosing different peaks in Fig. 3.

The time dependence of the field in the center of the fluctuation that will develop into an axiton for $A = 0.73$ is presented in Fig. 7, and for $A = 0.77$ in Fig. 8. In both cases the configuration collapses and the amplitude of θ rapidly increases in the center, even exceeding the value of π . This is followed by a period of several rebounds. An expanded view of the rebounds is shown in Fig. 9. During each rebound (eight in total in both cases) relativistic axions are emitted. We can see the signature of ax-

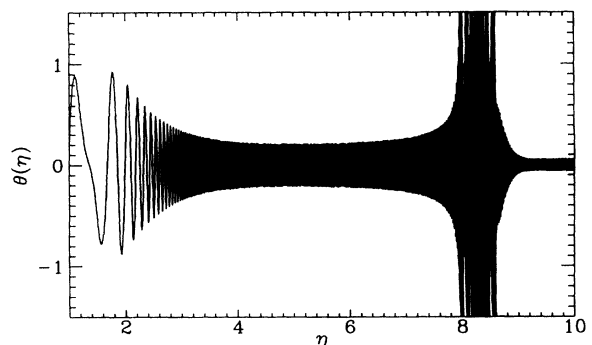


FIG. 7. The time dependence of θ in the center of an axiton in the (1+1)-dimensional calculation. The axiton was generated by the choice $A = 0.73$.

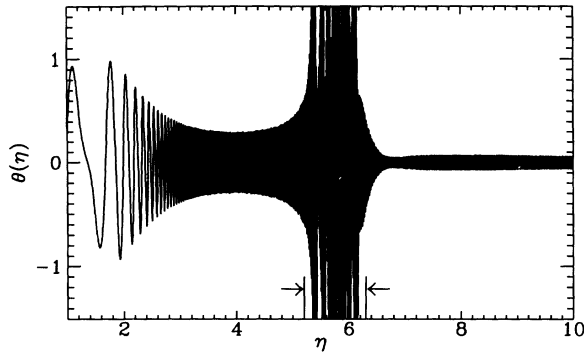


FIG. 8. The time dependence of θ in the center of an axiton in the (1+1)-dimensional calculation. The axiton was generated by the choice $A=0.77$.

ion emission by looking at the radial profile of an axiton. In Fig. 10 we show the profile of the axiton of Fig. 9 at three instants in time during one oscillation period. The emission of relativistic axions is seen in the outgoing waves of Fig. 10. The emission of relativistic axions reduces the energy of the central configuration below some critical value, at which point a pseudosoliton, an axiton, is produced.

The final energy density profile of this configuration for the case $A=0.77$ is shown in Fig. 11. At time $\eta=9$ (dotted line), outgoing secondary waves are still seen in the tail of the configuration. By time $\eta=11$ there is no evidence of outgoing radiation. The amplitude of the energy density at $r=0$ is 23.5, at $\eta=9$, and 12.9 at $\eta=11$ (the energy density in this graph is not normalized to the homogeneous background). It is clear that the energy density in the center scales as η^{-3} [e.g., $23.5/12.9=(11/9)^3$], confirming that the linear regime has been reached, the fluctuation is frozen, and the number of axions per comoving volume is conserved. The energy density of a homogeneous background at $\eta=10$ with $\eta_c=3.5$ and initial amplitude equal to the rms value of θ is 0.85 in the units of the figure. Thus, the fluctuation of Fig. 11 has an energy density contrast of 20.

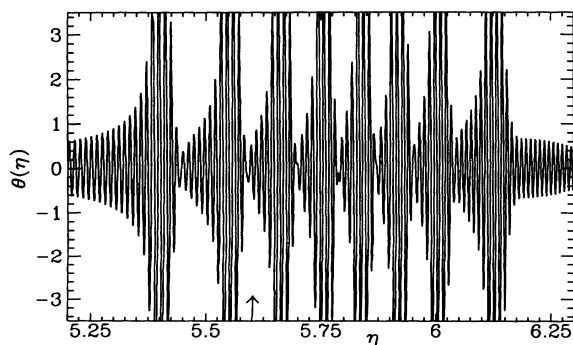


FIG. 9. An exploded view of the large amplitude oscillations in the center of the axiton of Fig. 8. The region pictured here is indicated by the arrows in Fig. 8.

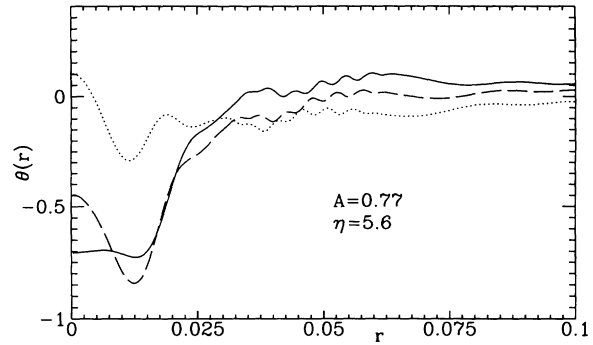


FIG. 10. The radial profile of the axiton of Fig. 9 at three instants during one period of oscillation around time $\eta=5.6$ indicated by the arrow in Fig. 9.

The radial coordinate r is the spherical analogy to x . At the values of η in Fig. 11 the axion mass has saturated to $m_a=3.5^{3.7}\eta \simeq 100\eta$. Therefore in the units of Fig. 11, the Compton wavelength of the axion is $0.01\eta^{-1}$, and the axiton is obviously much larger than m_a^{-1} —it is indeed a breatherlike configuration.

The axiton is a quasistable (on time scale m_a^{-1}) solution of the field equations in an expanding Universe. Since there are no absolutely stable spherically symmetric breatherlike solitons in flat space, in Minkowski space-time an axiton configuration will gradually decay anyway without the emission of axions present in the violent oscillations seen in Figs. 7 and 8. In an expanding Universe the situation is different. Once the axiton enters the linear regime density contrast becomes frozen by the cosmological expansion, and behaves as a clump of coherent field oscillations (or ultracold axions).

Not all fluctuations that pass through the nonlinear regime contract in physical space. For example, a sample spherical fluctuation for $A=0.70$ does not collapse. The corresponding energy density profiles of this fluctuation at two moments of time are presented in Fig. 12 by the dashed lines, which are the energy density profiles for a fluctuation

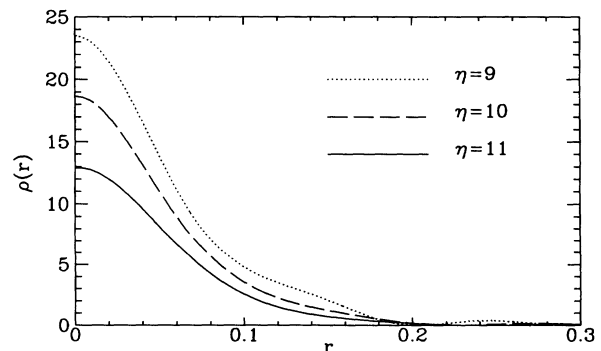


FIG. 11. Energy density profiles of the axiton in the spherically symmetric calculation with $A=0.77$ at three instants of time.

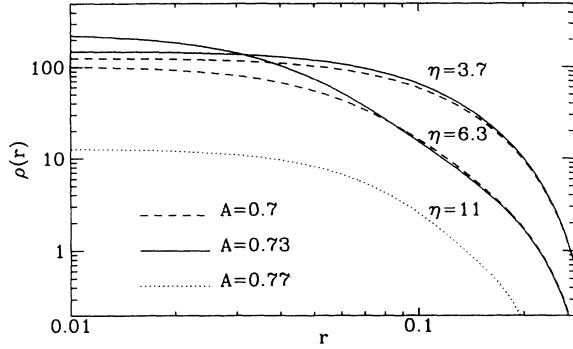


FIG. 12. Energy density profiles of three axitons in the spherically symmetric calculation. The axitons were generated by the choices $A=0.70$, $A=0.73$, and $A=0.77$. At $r \geq 0.1$ the curves separate into two pairs and a single configuration. The upper pair are the profiles at $\eta=3.4$, the next pair are the profiles at $\eta=6.3$, and the final dotted line is at $\eta=11$.

with $A=0.73$ which does undergo collapse. We see that the slope of the energy density in the nonlinear tail tends to a power law $\rho \propto r^{-3}$ prior to the collapse. This leads to an increase in field amplitude in the center, while, due to the overall expansion of the Universe, the amplitude decreases. For $A=0.73$, the first process wins for some period of time, see Fig. 7, while for $A=0.7$ the general expansion dominates, and the amplitude of the oscillations decreases monotonically. However, the decrease in amplitude is much slower than it would be with the harmonic potential, and the final energy density contrast with $\eta_c=3.5$ and $A=0.7$ is 45.

For comparison we also present in Fig. 12 the energy density profile of the fluctuation with $A=0.77$ at $\eta=11$. Remarkably, it has the same power-law slope, $\rho \propto r^{-3}$, despite the fact that this profile represents a fluctuation that has undergone “violent oscillations” accompanied by axion emission (see Figs. 8, 10, and 11).

Since the axion interaction is attractive, one can expect that bound states of axions can form. One example of such a bound state is the well-known “breather” solution in the (1+1)-dimensional sine-Gordon model. In 3+1 dimensions this solution possesses planar symmetry and turns out to be unstable with respect to fragmentation (we discuss this further in the next section). If a spherically symmetric counterpart of the “breather” would exist in Minkowski space-time, it would behave in an expanding Universe just as the fluctuation shown in Fig. 11. Thus the axiton is related to a spherically symmetric breather.

Suppose we can extrapolate these results to the range of realistic axion models, i.e., to larger values of η_c corresponding to smaller values of f_a . Then we must consider the possibility of producing enormous density contrasts. Indeed, both the increase in axion mass and the expansion of the Universe adiabatically decreases the amplitude of axion oscillations in the linear regime (or in the homogeneous state), so that at $T \lesssim \Lambda_{\text{QCD}}$ the corresponding background energy density is about $\bar{\rho}_a \approx T_{\text{eq}} T^3$, where

$T_{\text{eq}} \sim 5.5 \Omega_a h^2 \text{ eV}$ is the temperature of equal radiation and axion energy density. In the case of a collapsing nonlinear fluctuation, the final field configuration is the output of nonlinear dynamics. Let θ_L be the amplitude of field oscillations in the axiton at the time when it enters the linear regime at $T_L = T_1 / \eta_L$. Then the corresponding energy density in the fluctuation will be at this time about $\Lambda_a^4 \theta_L^2$. The ratio of the axiton energy density to the homogeneous background axion energy density will be

$$1 + \Phi \approx \Lambda_a^4 \theta_L^2 \eta_L^3 / T_{\text{eq}} T_1^3. \quad (3.8)$$

Using the results from Figs. 7 and 8 ($\theta_L \sim 0.1$ and $\eta_L > 6$),⁴ we obtain $1 + \Phi \approx 10^4$ prior to gravitational decoupling of the fluctuations from the cosmological expansion.

Although this possibility is exciting, a word of caution is necessary. Nonlinear dynamics is rather unpredictable, and one cannot exclude the possibility that at $\eta_c > 6$ all collapsing nonlinear fluctuations somehow dissipate, leaving very small θ_L . Note also that nonspherical configurations can evolve quite differently than the spherical configurations.

The range of initial conditions which will lead to monotonic behavior of the amplitude in the nonspherical case is expected to be wider. Our point of view is that spectrum of energy density contrasts can span the entire range from order 1 up to of order 10^4 or even larger. However, at this time we have nothing to say in regard to the number density of peaks as a function of its amplitude [18].

So far we have neglected the presence of other nonlinear structures which can be formed by the axion field during the QCD epoch, namely, axion domain walls and walls bounded by strings. We now turn to the question of their fate and their contribution to the dark matter distribution.

IV. AXION BREATHERS

In general, there are four sources of cosmic axions. The first source is thermal axions [19]. The second source, related to the initial misalignment of the axion degree of freedom from its true minimum, was discussed in the previous sections. We will refer to this source of axion energy density as the misalignment energy density. The third source is the decay of cosmic axion strings [20,21]. In Ref. [20] it was found that the energy density resulting from this process is 2 orders of magnitude larger than the misalignment energy density, while in the estimate of Ref. [21], the energy density from the decay of cosmic strings is comparable to the misalignment energy density. At $T \sim T_1$ the decay of strings will also produce an inhomogeneous axion field. While we cannot de-

⁴In any case, η_L will be larger than η_c , the value of η where the axion mass saturates to its zero-temperature value [see Eq. (3.7)], and $\eta_L > 6$ seems a very conservative estimate.

scribe the initial configuration emerging from string decay by the distribution of Eq. (3.6), we expect that the attractive nonlinear self-interaction will also play a role here, and the evolution will proceed along the lines described in Sec. III and will result in high density peaks. The fourth potential source of axions is related to the collisions and subsequent disappearance of axion domain walls. In this section we discuss this last process.

In most cases a network of vacuum domain walls is a cosmological disaster, since they soon come to dominate the energy density of the Universe [22]. Fortunately, in the $N=1$ axion model domain walls are effectively unstable and this problem is avoided.⁵ The process by which the domain walls disappear is through collisions of the string network with the walls. The usual assumption is that when a string loop (with a wall on the inside) hits a large wall the two pieces of wall annihilate and a vacuum hole is produced in the large wall. Since the surface energy of the hole is smaller than the surface energy of the wall, the vacuum hole expands and devours the wall. For an infinite domain wall there will be roughly one hole in the wall per Hubble radius, so in a couple of Hubble times the holes quickly overlap and the wall disappears. Domain walls of finite size (size smaller than the Hubble radius) form closed surfaces and shrink by themselves. An oversimplified point of view would be that all of the energy released in the disappearance of the domain walls is transferred to relativistic axions, which subsequently redshift away and would become an insignificant source of axion energy density. However, since the curvature and the width of the walls is of the order of the Hubble distance, one would presumably expect resulting axions to be only marginally relativistic upon unnihilation. The resulting axion density is estimated in Ref. [23].

Furthermore we shall argue here that the hole in a domain wall formed by a string-loop intersection is not vacuum, but rather consists of a bound state of two pieces of domain wall (which in the simplified scenario annihilated each other) corresponding to a generalization of the “breather” solution of the (1+1)-dimensional sine-Gordon model [24]. That is, the vacuum wall network is transformed into a breather wall network. The breather wall effectively evolves as a dust wall rather than a domain wall, so it represents cold dark matter.

We consider here the axion field in Minkowski space-time with planar symmetry as a function of two coordinates, time x_0 and one spatial direction, x_1 . It is convenient to introduce the dimensionless variables $t \equiv x_0 m_a$ and $z \equiv x_1 m_a$. The relevant breather solution to the equation of motion $\ddot{\theta} - \theta'' + \sin\theta = 0$ (overdot denotes d/dt and prime denotes d/dz) has the form [24]

$$\theta_v(t, z) = 4 \arctan \left[\frac{\sin(t/\tau)}{v \cosh(z/L)} \right], \quad (4.1)$$

where $\tau \equiv \sqrt{1+v^2}/v$ and $L \equiv \sqrt{1+v^2}$. One can interpret

this solution as a bound state of two static domain walls (or kinks), $\theta_{\text{kink}} = \pm 4 \arctan[\exp(z)]$. The free parameter v of the breather is related to the binding energy. Larger v corresponds to larger binding energy of the kinks. In terms of the spatial energy density distribution, the breather looks like a domain wall with an effective width L , but unlike the usual static domain wall, the field coherently oscillates with period τ in the breather. When $v \rightarrow 0$ the period tends to infinity, and when $v \rightarrow \infty$ the field oscillates with a frequency equal to the axion mass. The width of the breather scales in the opposite way with v : as $v \rightarrow 0$ the width is m_a^{-1} , and the width grows proportional to v at large v .

When considering wall-like structures, it is convenient to introduce a surface stress-energy tensor of the wall, $S_v^\mu \equiv \int_{-\infty}^{\infty} T_v^\mu dz$. While all the components of T_v^μ in the breather solution oscillate with time, the surface energy density is constant:

$$S_0^0 = 16f_a^2 m_a / \sqrt{1+v^2}, \quad (4.2)$$

and S_v^μ is a diagonal tensor. The spatial components of S_v^μ are oscillating functions. However, when considering the macroscopic properties of a wall, the relevant quantities are averages over an oscillation period. Upon averaging over an oscillation period $\langle S_z^z \rangle = 0$, as it must be for a wall of any nature [25]. For the time-averaged surface tension we find

$$\begin{aligned} \langle S_j^j \rangle &= 8f_a^2 m_a \left[2(\sqrt{1+v^2} - v) - \frac{v}{1+v^2} \right] \delta_j^j \\ &\equiv 8S_0^0 \delta_j^j. \end{aligned} \quad (4.3)$$

As $v \rightarrow 0$, the stress-energy tensor tends to the vacuum stress tensor, with $S_0^0 = S$, where S_0^0 is twice the energy density of a single kink. However, at large v , we have $S_0^0 \approx 16\Lambda_a^4/m_a v$ and $S \approx 8\Lambda_a^4/m_a v^3$. With increasing v , this tends to the stress-energy tensor of a dust shell. So in the expansion of the Universe the surface density of the breather wall has to decrease and v has to grow. Using Eqs. (4.2) and (4.3) we obtain, as a solution to the planar wall equations of motion [25],

$$S_0^0(R) = \frac{32f_a^2 m_a R^2}{R^4 + 1}, \quad (4.4)$$

where we assumed constant m_a and have normalized the scale factor in such a way that $R = 1$ at the moment when $v = 0$. Note that the number of axions per unit area is conserved at large R . Despite the fact that the breather is a bound state, its surface energy density decreases in expansion, exactly as the energy density of the solution presented in Fig. 11.

We can visualize the formation of the breather network in the following scenario. When domain walls form at $T \sim T_1$, every string loop develops a wall inside (an “antiloop” develops a wall outside). When a string hits a large segment of wall, the intersection region will not be empty, but will be a bound state of two domain walls. In the idealized approximation of planar symmetry, the

⁵The viewpoint of Ref. [3] suggests that $N > 1$ might be viable also since vacua might have different energies.

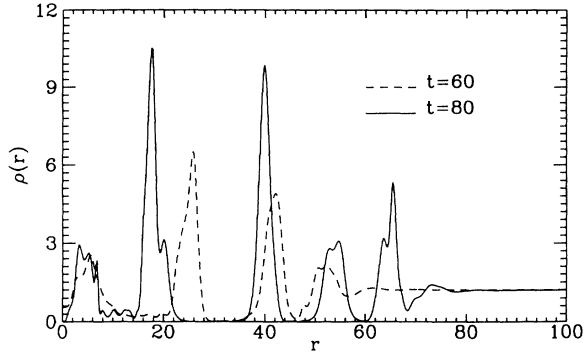


FIG. 13. The fragmentation of the breather.

bound state will correspond to the breather solution of Eq. (4.1). However, since the perfectly planar situation is unrealistic, the question arises whether breather walls are stable.

To answer this question we numerically integrated the axion equations of motion in Minkowski space-time with initial conditions corresponding to a perturbed breather wall. We evolved an axisymmetric configuration $\theta = \theta(t, z, r)$, which initially corresponded to the breather field distribution of Eq. (4.1) with $v = v(r)$. The value of v , and the corresponding pressure, was larger in the center [note that Eq. (4.3) corresponds to a system with negative pressure]. In a sense, this configuration corresponds to a bubble of new phase of lower energy density, and it is expected to expand. The question is whether the field inside the “bubble” will tend to a breather solution with a new constant value of v as the boundary of the bubble propagates outward. We have found that this does not occur: the breather wall is *unstable*. However, the energy density in the breather does not dissipate, but the breather fragments into clumps very similar to those discussed in Sec. III C. This result is not unexpected in view of the attractive nature of the axion self-interaction. The energy density profile in the r direction is presented in Fig. 13 at several moments of time.

Our conclusion in this section is that the decay of the axion domain wall network can provide yet another channel for axiton production in the axion distribution.

V. DISCUSSION

In principle, all axion miniclusters could be relevant to laboratory axion search experiments, since even for Φ as small as 1, the density is 10^{10} times larger than the local galactic halo density [see Eq. (2.3)]. Moreover, as we have noted already, the energy density in an axiton after it separates out from the general expansion will be Φ^4 times larger than the energy density at T_{eq} . For example, a rather moderate density contrast of $\Phi = 30$ at $\Lambda_{\text{QCD}} > T > T_{\text{eq}}$ will correspond to roughly an additional factor of 10^6 in the energy density of the axiton at $T \ll T_{\text{eq}}$.

We can define the boundary of future miniclusters as a surface where the density of the axiton becomes equal to its mean value. It turns out that, in our calculation, 80% of all axions belong to miniclusters at $\eta = 3$. See Fig. 3(b).

The probability of a direct encounter with a minicluster is small. Let us assume that all of the axions end up in miniclusters of mass $10^{-9} M_{\odot}$, density $10^{-14} \text{ g cm}^{-3}$, and radius $4 \times 10^{12} \text{ cm}$. Using a local halo mass density of $5 \times 10^{-25} \text{ g cm}^{-3}$ would give a minicluster number density of 7000000 pc^{-3} . With a typical velocity of 250 km s^{-1} the encounter rate would be 1 per 25 million years. Although the signal in an axion detector from a close encounter with a minicluster would be enormous, it might be a long wait. So the interesting question arises, could there be any other astrophysical consequences of very dense axion clumps? Below we shall discuss the possibility of “Bose star” formation in axion miniclusters.

The physical radius of an axiton at T_{eq} is larger by many orders of magnitude than the de Broglie wavelength of an axion in the corresponding gravitational well. Consequently, the gravitational collapse of the axion clump and subsequent virialization can be described in the usual terms of cold dark matter particles. In a few crossing times some equilibrium distribution (presumably close to an isothermal distribution) of axions in phase space will be established. It is remarkable that in spite of the apparent smallness of axion quartic self-couplings, $|\lambda_a| = (f_{\pi}/f_a)^4 \sim 10^{-53} f_{12}^{-4}$, the subsequent relaxation in an axion minicluster due to $2a \rightarrow 2a$ scattering can be significant as a consequence of the huge mean phase-space density of axions [12]. In the case of Bose-Einstein statistics the inverse relaxation time is $(1 + \bar{n})$ times the classical expression, or $\tau_R^{-1} \sim \bar{n} v_e \sigma \rho_a / m_a$, where σ is the corresponding cross section. For particles bound in a gravitational well, it is convenient to rewrite this expression in the form [12]

$$\tau_R \sim m_a^7 \lambda_a^{-2} \rho_a^{-2} v_e^2. \quad (5.1)$$

The shallower the gravitational well for a given density of axions, the larger the mean phase space density, and consequently the smaller the relaxation time due to the v_e^2 dependence in Eq. (5.1). Note also the dependence of the inverse relaxation time upon the square of the particle density.

The relaxation time (5.1) is smaller than the present age of the Universe if the energy density in the minicluster satisfies

$$\rho_{10} > 10^6 v_{-8} \sqrt{f_{12}}, \quad (5.2)$$

where $\rho_{10} \equiv \rho / (10 \text{ eV})^4$ and $v_{-8} \equiv v_e / 10^{-8}$. If this occurs, then an even denser core in the center of the axion cloud should start to form. An analogous process is the so-called gravithermal instability caused by gravitational scattering. This was studied in detail for star clusters, where the “particles” obey classical Maxwell-Boltzmann statistics. Axions will obey Bose-Einstein statistics, with equilibrium phase-space density $n(p) = n_{\text{cond}} + [e^{\beta E} - 1]^{-1}$, containing a sum of two contributions, a Bose condensate and a thermal distribution. The maximum energy density that noncondensed axions can saturate is $\rho_{\text{ther}} \sim m_a^4 v_e^3$, which corresponds to $\bar{n}_{\text{ther}} \sim 1$. Consequently, given the initial condition $\bar{n} \gg 1$, one expects that eventually the number of particles in the condensate will be comparable to the total number of

particles in the region if relaxation is efficient. Under the influence of self-gravity, a Bose star [17,26,27] then forms [12]. One can consider a Bose star as coherent axion field in a gravitational well, generally with nonzero angular momentum [17].

Comparing Eqs. (2.3) and (5.2), we conclude that the relaxation time is smaller than the present age of the Universe and conditions for Bose star formation can be reached in miniclusters with a density contrast $\Phi \gtrsim 30$ at the QCD epoch.

Under appropriate conditions stimulated decays of axions to two photons in a dense axion Bose star are possible [17,28] (see also [29]), which can lead to the formation of unique radio sources—axionic masers. In view of the results of this paper we conclude that the questions of axion Bose star formation, structure, and possible astrophysical signatures deserve detailed study.

In conclusion, we have presented a three-dimensional

numerical study of the evolution of inhomogeneities in the axion field around the QCD epoch, including for the first time important nonlinear effects. We found that the nonlinear effects of the attractive self-interaction can lead to a much larger density of axions in miniclusters than previously estimated. Large amplitude density contrasts form solitons we call axitons, and resemble the bound-state “breather” solutions of the (1+1)-dimensional sine-Gordon model. The increase in the axion density may be sufficiently large that axion miniclusters formed by the fluctuations might exceed the critical density necessary for them to relax to form Bose stars.

ACKNOWLEDGMENTS

E.W.K. and I.I.T. were supported by the DOE and NASA under Grant No. NAGW-2381.

-
- [1] R. D. Peccei and H. Quinn, *Phys. Rev. Lett.* **38**, 1440 (1977); *Phys. Rev. D* **16**, 1791 (1977); S. Weinberg, *Phys. Rev. Lett.* **40**, 223 (1978); F. Wilczek, *ibid.* **40**, 279 (1978).
- [2] Other solutions to the strong *CP* problem include vanishing of a quark mass, see, e.g., D. B. Kaplan and A. Manohar, *Phys. Rev. Lett.* **56**, 2004 (1986); models where an otherwise exact *CP* is either softly or spontaneously broken, see A. Nelson, *Phys. Lett.* **136B**, 387 (1984); S. M. Barr, *Phys. Rev. Lett.* **53**, 329 (1984); or through the action of wormholes, see B. Nielsen and M. Ninomiya, *ibid.* **62**, 1429 (1989); K. Choi and R. Holman, *ibid.* **62**, 2575 (1989); J. Preskill, S. P. Trivedi, and M. Wise, *Phys. Lett. B* **223**, 26 (1989).
- [3] R. Holman, S. H. Hsu, T. W. Kephart, E. W. Kolb, R. Watkins, and L. M. Widrow, *Phys. Lett. B* **282**, 132 (1992); S. Barr and D. Seckel, *Phys. Rev. D* **46**, 539 (1992); M. Kamionkowski and J. March-Russell, *Phys. Lett. B* **282**, 137 (1992).
- [4] D. Dicus, E. Kolb, V. Teplitz, and R. Wagoner, *Phys. Rev. D* **18**, 1829 (1978); **22**, 839 (1980); M. Fukugita, S. Watamura, and M. Yoshimura, *Phys. Rev. Lett.* **48**, 1522 (1982); *Phys. Rev. D* **26**, 1840 (1982).
- [5] G. Raffelt and D. Seckel, *Phys. Rev. Lett.* **60**, 1793 (1988); M. S. Turner, *ibid.* **60**, 1797 (1988); R. Mayle *et al.*, *Phys. Lett. B* **203**, 188 (1988); T. Hatsuda and M. Yoshimura, *ibid.* **203**, 469 (1988).
- [6] J. Preskill, M. Wise, and F. Wilczek, *Phys. Lett.* **120B**, 127 (1983); L. F. Abbott and P. Sikivie, *ibid.* **120B**, 133 (1983); M. Dine and W. Fischler, *ibid.* **120B**, 137 (1983).
- [7] For recent reviews, see M. S. Turner, *Phys. Rep.* **197**, 67 (1990); G. G. Raffelt, *ibid.* **198**, 1 (1990).
- [8] M. S. Turner, *Phys. Rev. D* **33**, 889 (1986).
- [9] C. J. Hogan and M. J. Rees, *Phys. Lett. B* **205**, 228 (1988).
- [10] P. Sikivie, *Phys. Rev. Lett.* **51**, 1415 (1983).
- [11] E. Kolb and I. I. Tkachev, *Phys. Rev. Lett.* **71**, 3051 (1993).
- [12] I. I. Tkachev, *Phys. Lett. B* **261**, 289 (1991).
- [13] D. Gross, R. Pisarski, and L. Yaffe, *Rev. Mod. Phys.* **53**, 43 (1981).
- [14] This does not necessarily require the reheating temperature after inflation to be higher than f_a , since inflation itself can produce strong fluctuations in the axion field as discussed by A. D. Linde and D. H. Lyth, *Phys. Lett. B* **246**, 353 (1990); D. H. Lyth and E. D. Stewart, *Phys. Rev. D* **46**, 532 (1992).
- [15] E. W. Kolb and M. S. Turner, *The Early Universe* (Addison-Wesley, Redwood City, CA, 1990).
- [16] D. H. Lyth, *Phys. Rev. D* **45**, 3394 (1992).
- [17] I. I. Tkachev, *Pis'ma Astron. Zh.* **12**, 726 (1986) [*Sov. Astron. Lett.* **12**, 305 (1986)].
- [18] Another consideration is that a typical minicluster mass is $10^{-9}M_\odot$. If axions are the dark matter in our Galaxy, then there can be of order 10^{20} miniclusters in our Galaxy. Even if we have been too optimistic by several orders of magnitude about the probability of initial configurations that lead to large density contrasts, there will still be a sizable number of them in our Galaxy.
- [19] For a discussion of thermal axion production, see [15].
- [20] R. Davis, *Phys. Lett. B* **180**, 225 (1986).
- [21] D. Harari and P. Sikivie, *Phys. Lett. B* **195**, 361 (1987).
- [22] M. B. Voloshin, I. Yu. Kobzarev, and L. B. Okun', *Yad. Fiz.* **20**, 1229 (1974) [*Sov. J. Nucl. Phys.* **20**, 644 (1975)].
- [23] D. H. Lyth, *Phys. Lett. B* **275**, 279 (1992).
- [24] R. Rajaraman, *Solitons and Instantons* (Elsevier Science, New York, 1982).
- [25] V. A. Berezhin, V. A. Kuzmin, and I. I. Tkachev, *Phys. Rev. D* **26**, 2919 (1987).
- [26] R. Ruffini and S. Bonazzola, *Phys. Rev.* **187**, 1767 (1969); J. D. Breit, S. Gupta, and A. Zaks, *Phys. Lett.* **140B**, 329 (1984); M. Gleiser, *Phys. Rev. D* **38**, 2376 (1988); P. Jetzer, *Nucl. Phys.* **B316**, 411 (1989).
- [27] E. Seidel and W.-M. Suen, *Phys. Rev. Lett.* **66**, 1659 (1991).
- [28] I. I. Tkachev, *Phys. Lett. B* **191**, 41 (1987).
- [29] T. W. Kephart and T. J. Weiler, Report No. VAND-TH-90-2, 1990 (unpublished).

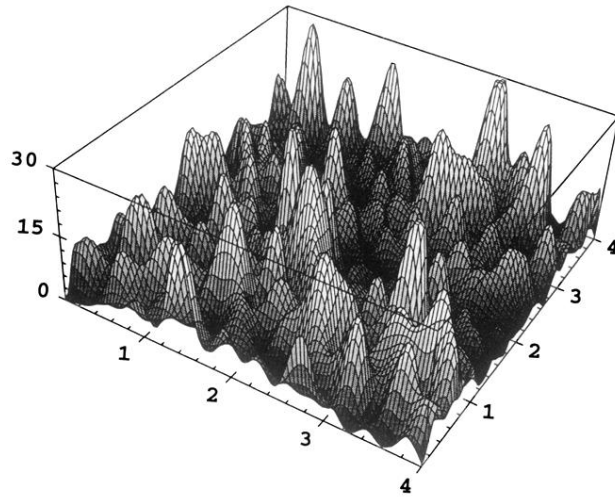


FIG. 1. A two-dimensional slice through the three-dimensional initial conditions for the axion field evolution. The time is $\eta=0.4$. In the units shown in the figure the Hubble radius at this time is 0.4 units and the inverse of the axion mass is 75 units. The height of the figure corresponds to the energy density in the axion field: $\rho_a(\eta) \times \eta^4 / \bar{\rho}_a(\eta=3)$.

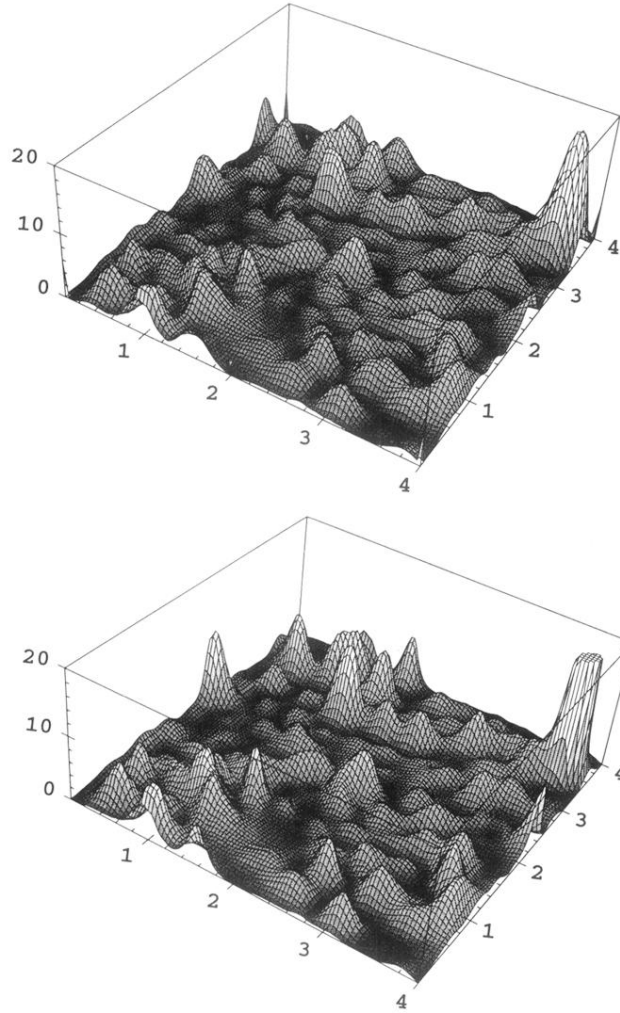


FIG. 2. A two-dimensional slice through the three-dimensional box at time corresponding to $\eta=2$ for the harmonic potential (top) and the axion potential (lower). The Hubble radius at this time is 2 units and the inverse of the axion mass is 0.038 units. The height of the figure corresponds to the energy density in the axion field normalized to the height for homogeneous field evolution: $\rho_a(\eta=2)/\bar{\rho}_a(\eta=2)$.

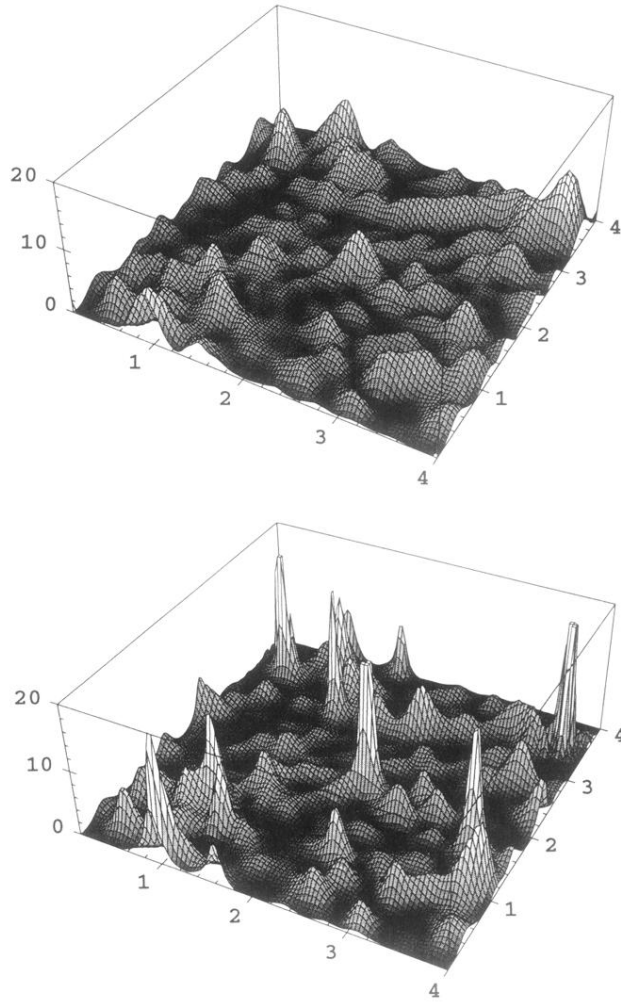


FIG. 3. A two-dimensional slice through the three-dimensional box at time corresponding to $\eta=3$ for the harmonic potential (top) and the axion potential (lower). The Hubble radius at this time is 3 units and the inverse of the axion mass is 0.005 units. The height of the figure corresponds to the energy density in the axion field normalized to the height for homogeneous field evolution: $\rho_a(\eta=3)/\bar{\rho}_a(\eta=3)$.

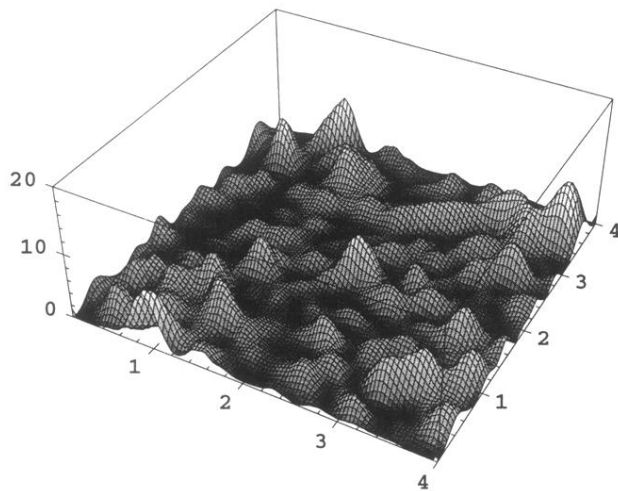


FIG. 4. A two-dimensional slice through the three-dimensional box at time corresponding to $\eta=4$ for the harmonic potential. The Hubble radius at this time is 4 units and the inverse of the axion mass is 0.0015 units. The height of the figure corresponds to the energy density in the axion field normalized to the height for homogeneous field evolution: $\rho_a(\eta=4)/\bar{\rho}_a(\eta=4)$.

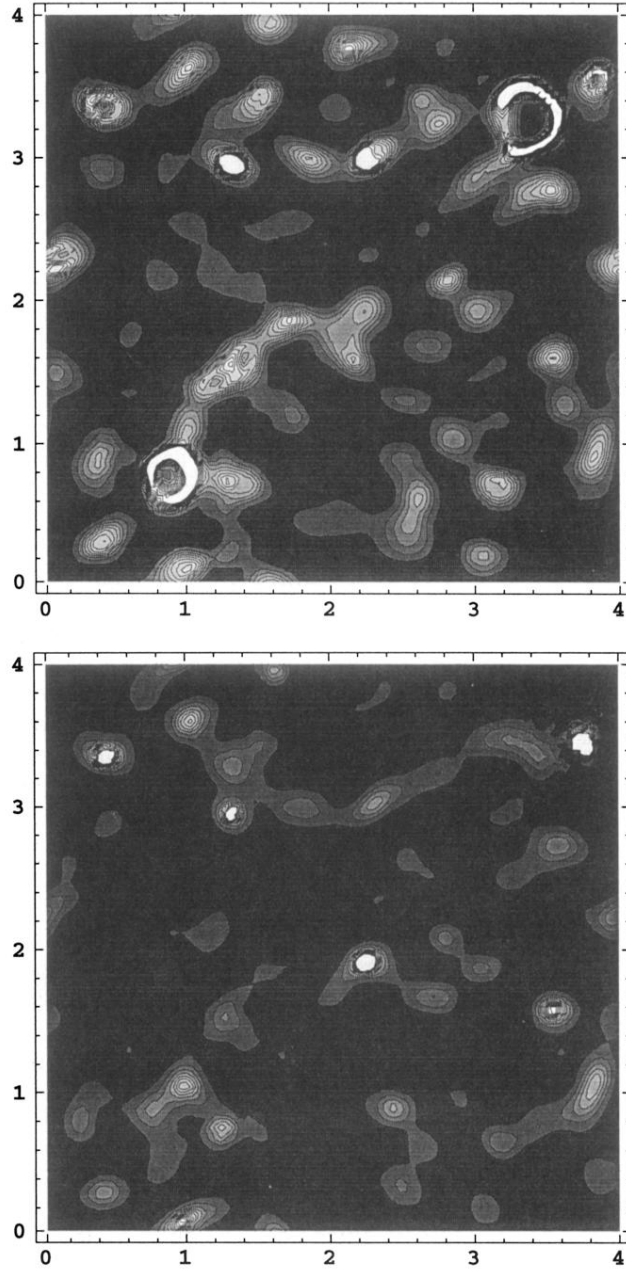


FIG. 5. A two-dimensional slice through the three-dimensional box. White regions correspond to high density. The upper figure is for $A=2$ at time corresponding to $\eta=2$ and the lower figure is for $A=1$ at $\eta=3$ [i.e., the same as in Fig. 3(b)].

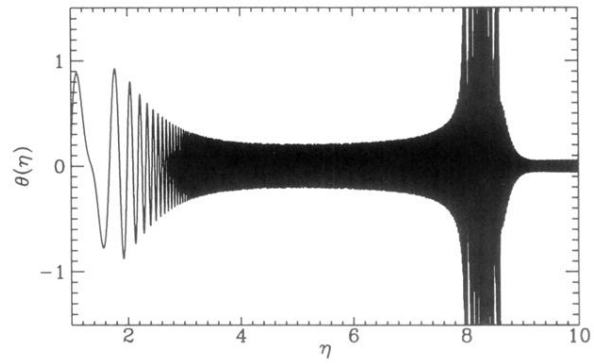


FIG. 7. The time dependence of θ in the center of an axiton in the (1+1)-dimensional calculation. The axiton was generated by the choice $A=0.73$.

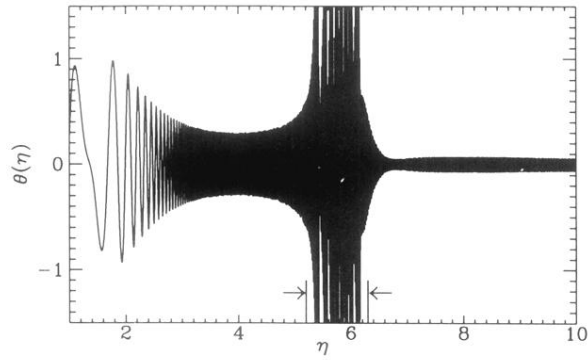


FIG. 8. The time dependence of θ in the center of an axiton in the (1+1)-dimensional calculation. The axiton was generated by the choice $A = 0.77$.

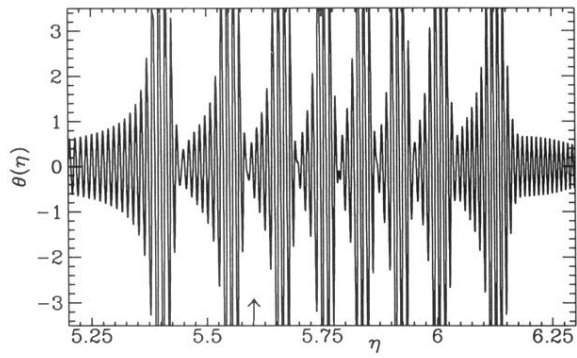


FIG. 9. An exploded view of the large amplitude oscillations in the center of the axiton of Fig. 8. The region pictured here is indicated by the arrows in Fig. 8.